

Lifetimes of low-lying excited states in ${}^{86}_{36}\text{Kr}_{50}$

J. Henderson,^{1,2,*} A. Chester,³ G. C. Ball,² R. Caballero-Folch,²
 T. Domingo,³ T. E. Drake,⁴ L. J. Evitts,^{2,5} G. Hackman,² S. Hallam,^{2,5,†}
 A. B. Garnsworthy,² M. Moukaddam,^{2,†} P. Ruotsalainen,^{2,‡} J. Smallcombe,²
 J. K. Smith,^{2,§} K. Starosta,^{3,¶} C. E. Svensson,⁶ and J. Williams³

¹*Lawrence Livermore National Laboratory, Livermore, CA 94550, USA*

²*TRIUMF, Vancouver BC Canada V6T 2A3*

³*Department of Chemistry, Simon Fraser University, Burnaby, BC V5A 1S6, Canada*

⁴*Department of Physics, University of Toronto,
 Toronto, Ontario M5S 1A7, Canada*

⁵*Department of Physics, University of Surrey,
 Guildford, GU2 7XH, United Kingdom*

⁶*Department of Physics, University of Guelph, Guelph, ON N1G 2W1, Canada*

(Dated: November 5, 2018)

Abstract

Background: The evolution of nuclear magic numbers at extremes of isospin is a topic at the forefront of contemporary nuclear physics. $N = 50$ is a prime example, with increasing experimental data coming to light on potentially doubly-magic ^{100}Sn and ^{78}Ni at the proton-rich and proton-deficient extremes, respectively.

Purpose: Experimental discrepancies exist in the data for less exotic systems. In ^{86}Kr the $B(E2; 2_1^+ \rightarrow 0_1^+)$ value - a key indicator of shell evolution - has been experimentally determined by two different methodologies, with the results deviating by 3σ . Here, we report on a new high-precision measurement of this value, as well as the first measured lifetimes and hence transition strengths for the 2_2^+ and $3_{(2)}^-$ states in the nucleus.

Methods: The Doppler-shift attenuation method was implemented using the TIGRESS gamma-ray spectrometer and TIGRESS integrated plunger (TIP) device. High-statistics Monte-Carlo simulations were utilized to extract lifetimes in accordance with state-of-the-art methodologies.

Results: Lifetimes of $\tau(2_1^+) = 336 \pm 4(\text{stat.}) \pm 20(\text{sys.})$ fs, $\tau(2_2^+) = 263 \pm 9(\text{stat.}) \pm 19(\text{sys.})$ fs and $\tau(3_{(2)}^-) = 73 \pm 6(\text{stat.}) \pm 32(\text{sys.})$ fs were extracted. This yields a transition strength for the first-excited state of $B(E2; 2_1^+ \rightarrow 0^+) = 259 \pm 3(\text{stat.}) \pm 16(\text{sys.})$ e²fm⁴.

Conclusions: The measured lifetime disagrees with the previous Doppler-shift attenuation method measurement by more than 3σ , while agreeing well with a previous value extracted from Coulomb excitation. The newly extracted $B(E2; 2_1^+ \rightarrow 0_1^+)$ value indicates a more sudden reduction in collectivity in the $N = 50$ isotones approaching $Z = 40$.

* henderson64@llnl.gov

† Present address: Department of Physics, University of Surrey, Guildford, GU2 7XH, United Kingdom

‡ Present address: Department of Physics, University of Jyväskylä, FIN-40014 Finland

§ Present address: Physics Department, Reed College, Portland OR, 97202, USA

¶ starosta@sfu.ca

I. INTRODUCTION

Determining the evolution of the nuclear magic-numbers far from the line of β -stability is the subject of much experimental and theoretical effort. In particular, the advent of the next generation of radioactive ion beam facilities presents the promise of further study of this evolution at the extremes of isospin. So-called “islands of inversion” are now well established at $N = 8$, $N = 20$ and $N = 28$ [1–3], all of which are established major shell-closures at the line of stability, as well as the sub-shell closure at $N = 40$ [4]. The $N = 50$ shell may also be expected to exhibit a similar breakdown of the nominal magic numbers (see e.g. [5, 6]), incorporating the neutron-deficient (nominally) doubly-magic ^{100}Sn and neutron-rich ^{78}Ni . Key experimental observables in the mapping of nuclear shell evolution include excited 2_1^+ state energies and $E2$ transition strengths ($B(E2; 2^+ \rightarrow 0^+)$). In order to properly assess the evolution of nuclear shell closures the experimental determination of these observables at stability where “normal” configurations dominate is thus important.

Of the even-even $N = 50$ isotones, $B(E2; 2_1^+ \rightarrow 0_1^+)$ data is available for seven nuclides, from ^{80}Zn through to ^{92}Mo . A clear minimum is found for ^{90}Zr , which has $Z = 40$ corresponding to a sub-shell closure and behaves very much like a doubly-magic nucleus. Between $Z = 30$ and $Z = 38$, the $B(E2)$ values are relatively consistent, while the data for heavier isotones is limited to ^{92}Mo , preventing any systematic comparison. The data for $^{86}_{36}\text{Kr}$ is found to be inconsistent, with $B(E2)$ values determined from a lifetime measurement using the DSAM technique [7] found to deviate from that determined using Coulomb excitation [8] at a 3σ level. In the event that the $B(E2)$ value extracted from DSAM in Ref. [7] is correct, the degree of collectivity characterized by the $B(E2)$ decreases steadily from a maximum at ^{82}Ge towards the minimum at ^{90}Zr . If, on the other hand, the Coulomb-excitation $B(E2)$ of Ref. [8] is correct, the decrease is rather more pronounced from a near-maximum at $Z = 36$ to a minimum at $Z = 40$. A figure showing $N = 50$ $B(E2; 2_1^+ \rightarrow 0_1^+)$ systematics is shown in the discussion section of this paper.

In the present work, we therefore undertook to remeasure the lifetime of the 2_1^+ state in ^{86}Kr using the DSAM technique, following population by unsafe Coulomb-excitation. The major benefit of this population mechanism is that Coulomb excitation cross-sections reduce as one requires more excitation energy or further steps of excitation, greatly reducing the impact of feeding from higher lying states on the lifetimes measured for the states of

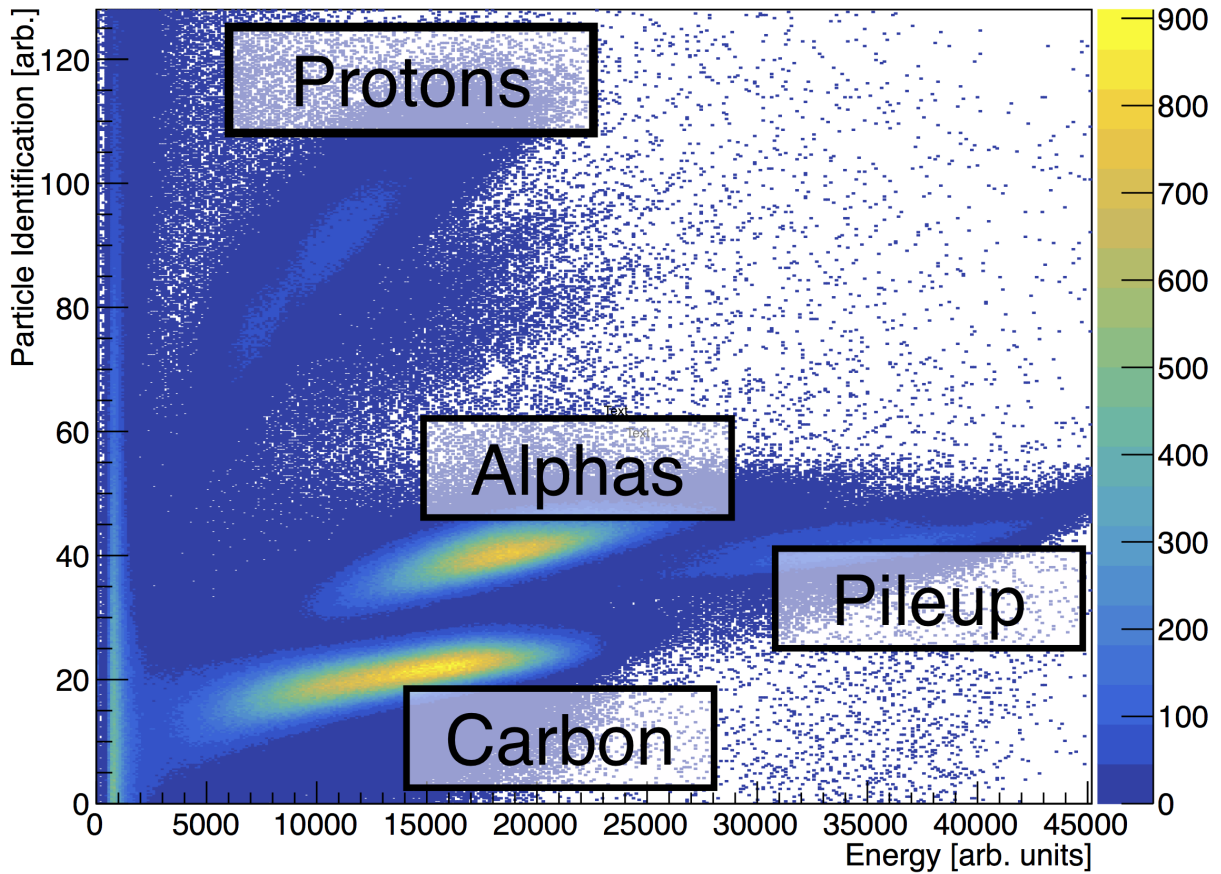


FIG. 1. The particle identification (PID) parameter determined from waveform fitting plotted against the energy in the CsI(Tl) detectors with the major loci indicated.

interest. A benefit for the present measurement over that of Ref. [7] is the use of a 4π HPGe array, greatly enhancing sensitivity to near-degenerate states which might only be resolved at either forward- or backward angles. The analysis of this work is very similar to that described in Ref. [9] but utilizes the DSAM technique rather than the recoil-distance method.

II. EXPERIMENTAL DETAILS

States of interest were populated through the unsafe Coulomb excitation of ^{86}Kr in inverse kinematics. A beam of ^{86}Kr ions was produced by the TRIUMF offline ion source [10], accelerated to 256.7 MeV by the TRIUMF-ISAC accelerator chain and delivered to the TRIUMF-ISAC gamma-ray escape-suppressed spectrometer (TIGRESS) facility [11]. For

the present measurement, TIGRESS contained eleven 32-fold segmented HPGe clover detectors, with three located at 45° , five at 90° and three at 135° relative to the beam axis. TIGRESS surrounded the TIGRESS integrated plunger (TIP) [12] setup which consisted of a wall of $24 \times 16 \times 14 \text{ mm}^2$, 2-mm thick CsI(Tl) detectors located 51.7 mm downstream of the target. The beam was impinged onto a $2.165\text{-}\mu\text{m}$ (0.5-mg/cm^2) thick amorphous carbon target, backed by a $14.917\text{-}\mu\text{m}$ (28.8-mg/cm^2) thick gold foil to stop the beam-like particles [13]. A beam intensity of approximately 100 ppA was maintained for 30 hours. Data were acquired using the TIGRESS digital data acquisition system [14] with a particle- γ coincidence condition required. Detector waveforms were collected for both the HPGe and CsI(Tl) detectors, as well as coincident accelerator-RF waveforms. A similar experimental configuration using TIP, TIGRESS and the same target used in the present work is discussed in Ref. [15].

III. ANALYSIS

Data were unpacked and analyzed using the in-house GRSISort analysis software [16], built on the ROOT framework [17]. Events were constructed on the basis of a trigger ID, provided by the TIGRESS acquisition system. Precise relative timing information was extracted through the fitting of the CsI(Tl), HPGe and RF waveforms. Particle- γ pairs were constructed on the basis of this timing information which were themselves coincident with an RF pulse and, thus, a beam bucket from the accelerator chain. Waveform fitting also allowed for particle identification (PID) on the basis of the well-understood response of CsI(Tl) (see, e.g. Ref. [12]). A PID plot for the innermost four CsI(Tl) detectors is shown in Fig. 1.

In order to maximize peak-to-background, HPGe signals were added back on the basis of both the time of the detection event and the sub-clover position provided by the segmented detector anodes. The added-back data were then time gated on the basis of both an RF beam bucket and a time-coincident CsI(Tl) detector hit. Finally, a PID gate was applied, requiring the coincident CsI(Tl) event to be consistent with a carbon recoil. The γ -ray gating process is shown in Fig. 2. The consequence of this series of filters was a very clean γ -ray spectrum. Some time-random β decay lines remain in the spectrum, however these do not interfere with the DSAM lineshape analysis. The only discernible background arising

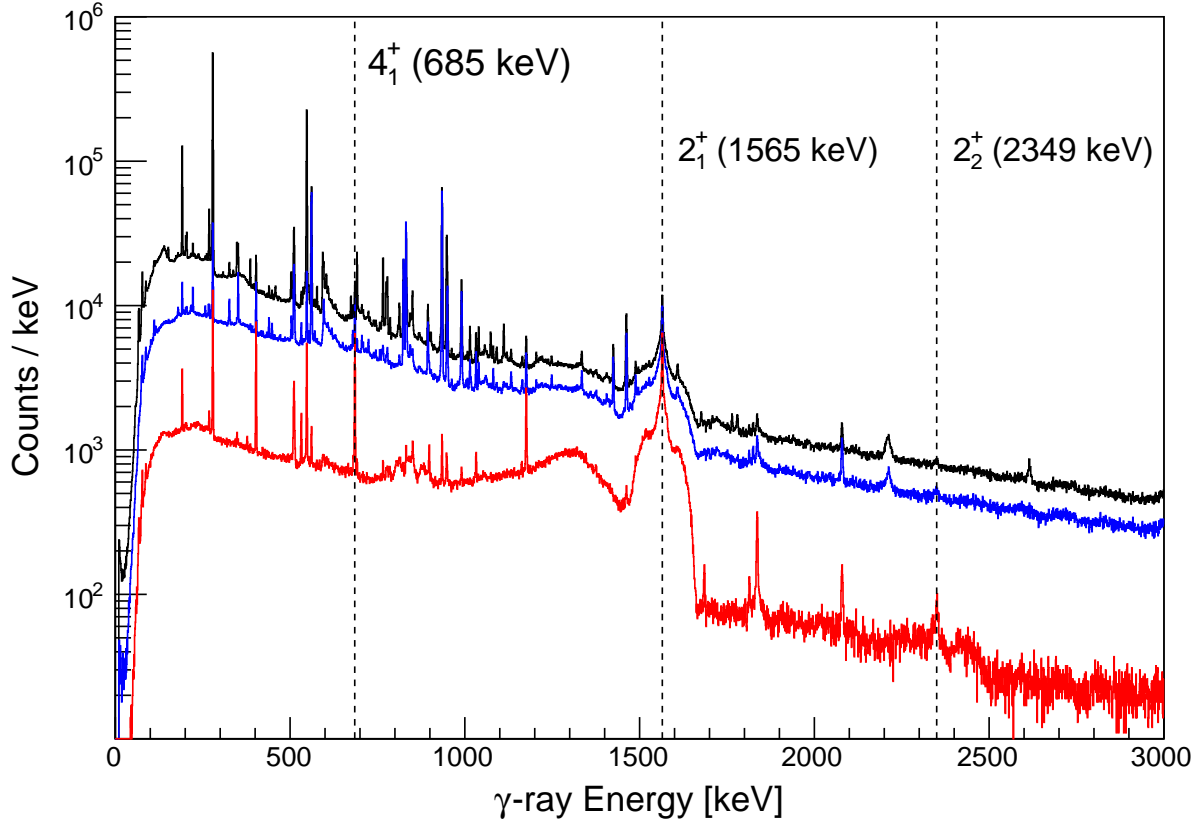


FIG. 2. Black: Addback γ -ray spectrum. Blue: Requiring a good time coincidence with a CsI(Tl) event and an RF beam bucket. Red: Requiring the coincident CsI(Tl) event that has a PID parameter consistent with the a carbon detection. γ -ray peaks arising from the decays of states of interest are indicated. Note that γ -rays originating from the 3^- state are not resolvable from the those from the 2_1^+ state in this figure.

from in-flight decays (i.e. not the result of time-random β decays) were weak γ -ray lines consistent with a single-proton transfer reaction into ^{87}Rb , the isotonic neighbour of ^{86}Kr . Where resolvable these weak lines were fitted with a simple Gaussian and included in fitting of the Monte-Carlo simulations. No strong background lines were observed to interfere with the decays which will be discussed.

Observed in the data were four transitions from the decay of excited states of ^{86}Kr : $2_1^+ \rightarrow 0_1^+$ ($E_\gamma = 1564.67$ keV), $4_1^+ \rightarrow 2_1^+$ ($E_\gamma = 685.35$ keV), $2_2^+ \rightarrow 0_1^+$ ($E_\gamma = 2349.47$ keV) and $3_{(2)}^- \rightarrow 2_1^+$ ($E_\gamma = 1534.24$ keV). Of these transitions, only the $4_1^+ \rightarrow 2_1^+$ had no in-flight lineshape component, consistent with its previously determined halflife of 3.1 ns. The re-

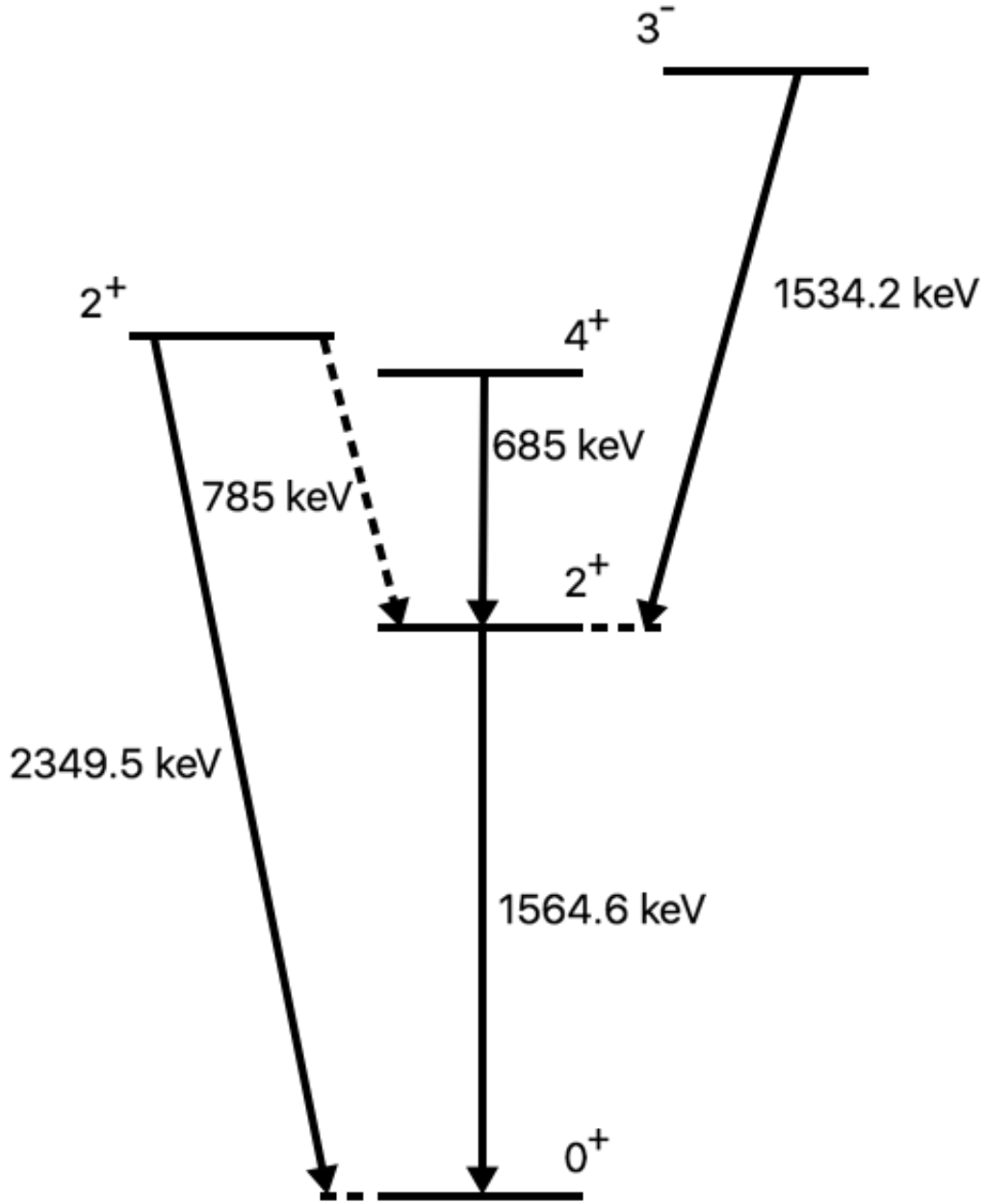


FIG. 3. Reduced level scheme indicating the states of interest in the present work. Dashed transitions indicate γ rays that were not observed but were incorporated into the lineshape analysis.

maining three transitions were thus suitable for a Doppler-shift attenuation method (DSAM) analysis. A reduced level scheme showing the states observed in the present work is given in Fig. 3.

The techniques used to analyze the DSAM spectra are outlined in detail in Ref. [9] and Ref. [18]. High-statistics GEANT4 simulations were performed using a detailed model

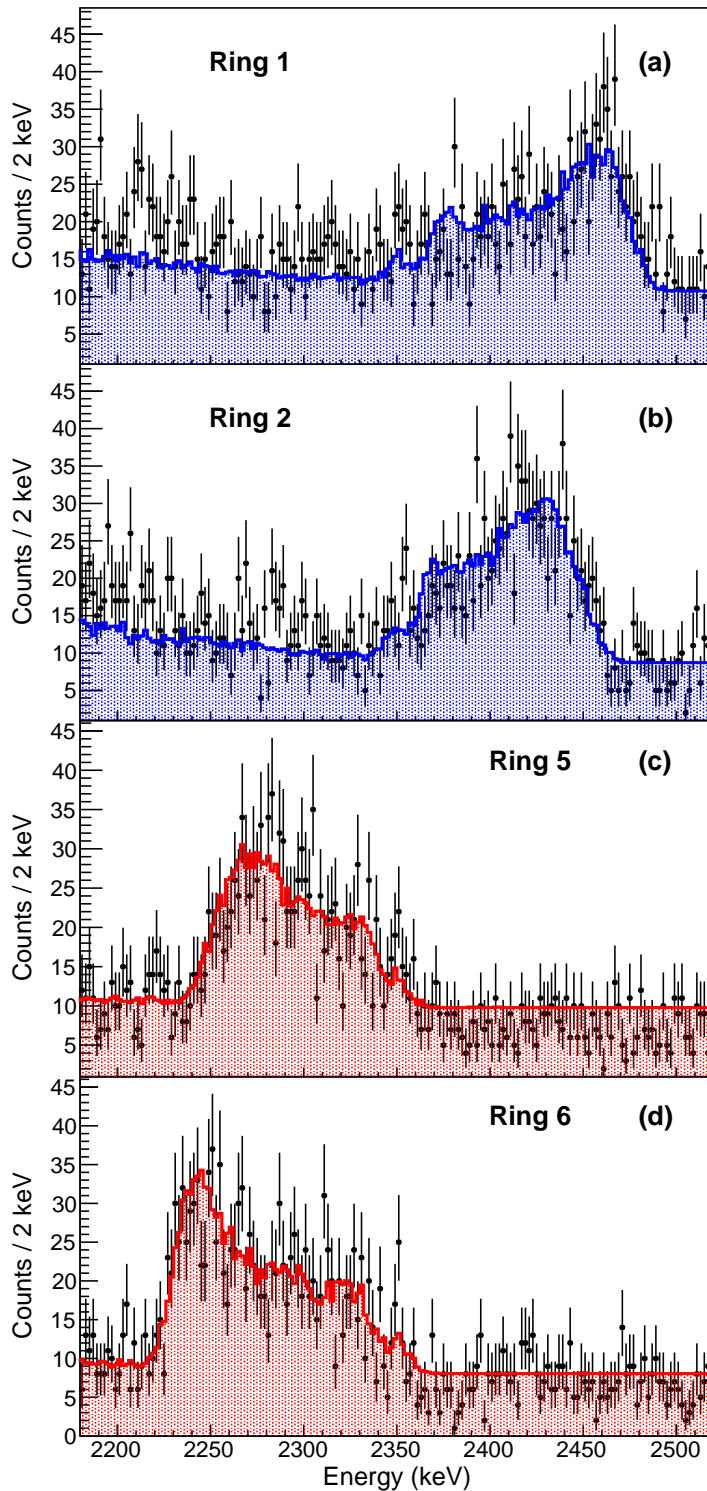


FIG. 4. Simulated lineshape (filled) plotted along with the experimental data (data points) for rings 1, 2, 5 and 6 (a-d) for a simulated lifetime, $\tau(2_2^+) = 260$ fs.

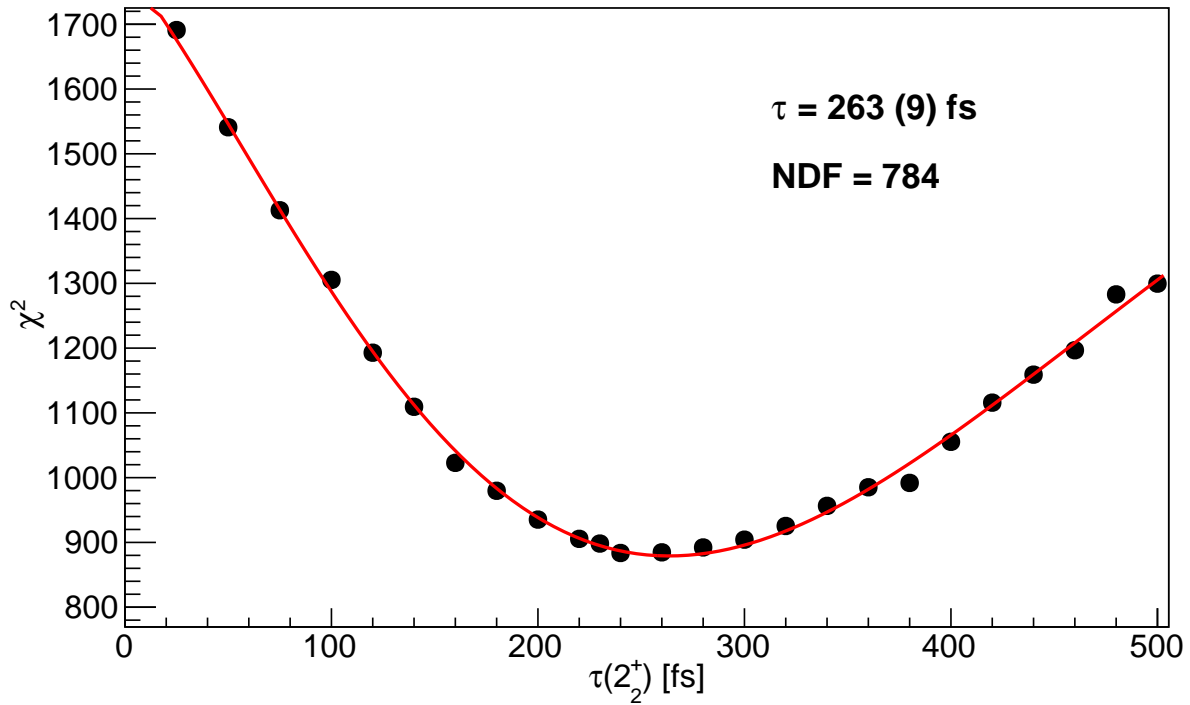


FIG. 5. χ^2 plotted against the simulated lifetime of the 2_2^+ state for all four sensitive rings (see Fig. 4). As indicated, the χ^2 minimum is found to correspond to $\tau = 263$ (9) fs. Once systematic uncertainties are incorporated the final value becomes $\tau = 263$ (9) (19) fs.

of the TIGRESS and TIP spectrometers. For the purposes of the DSAM analysis, only the inner eight TIP CsI(Tl) detectors were used - for the remaining detectors the particle-identification plot (see Fig. 1) did not give good separation for the carbon nuclei, and losses due to thresholds could not be consistently accounted for. The simulated GEANT4 spectra were smeared according to the observed HPGe detector resolution prior to comparisons with the experimental data. For comparison with simulations, TIGRESS was separated into six rings corresponding to the downstream- and upstream-most rings of the 45° , 90° and 135° clovers, with ring 1 being the most downstream and ring 6 the most upstream. No sensitivity to lifetimes was found for the rings about 90° . Angular correlation effects were not found to be important and were not included in the further analysis.

A. The $2_2^+ \rightarrow 0_1^+$ transition

The $2_2^+ \rightarrow 0_1^+$ ($E_\gamma = 2349$ keV) transition was well separated from the other lines and could thus be analyzed independently. No feeding transition to the 2_1^+ state was observed ($E_\gamma = 749$ keV), however this would not be expected to be visible above background. Simulated spectra were constructed from $5 \cdot 10^6$ CsI(Tl)-HPGe coincidences. The spectra were then fit to the experimental data for all four sensitive rings (1, 2, 5 & 6) simultaneously. The parameters in the fits were a scaling parameter, a zeroth-order polynomial background which was constrained (but not fixed) prior to the fit, and an E_γ -shift parameter to account for any low-level mismatch between the simulated and experimental energies - in particular to allow for binning effects. Due to the low level of statistics for this transition, the use of a maximum-likelihood method was essential, as described in Ref. [9]. The simulated lineshape corresponding to the maximized log-likelihood is shown in Fig. 4. To account for the fact that the reduced $\chi_{\min}^2/\nu = 1.12 > 1$, the statistical uncertainties were inflated by a factor of $\sqrt{\chi_{\min}^2/\nu} = 1.06$ following the prescription of Ref. [19], yielding a final lifetime of 263 fs with $\delta\tau_{\text{stat}} = 9$ fs.

B. The $2_1^+ \rightarrow 0_1^+$ and $3_{(2)}^- \rightarrow 2_1^+$ transitions

The $2_1^+ \rightarrow 0_1^+$ (1564 keV) and $3_{(2)}^- \rightarrow 2_1^+$ (1534 keV) transitions lie too close in energy for their respective lineshapes to be fully disentangled. Indeed, in the downstream (rings 1 and 2) data, the $3_{(2)}^- \rightarrow 2_1^+$ transition could not be visually identified. Consequently, and because the $3_{(2)}^- \rightarrow 2_1^+$ transition feeds the 2_1^+ state, the two transitions had to be analyzed simultaneously. No indication for any competing branch in the decay of the $3_{(2)}^-$ state was observed, nor is there any indication of such a decay in the literature. The branch was therefore assumed to be 100 % in the present work. This is consistent with the literature $B(E3; 3^- \rightarrow 0^+)$ value extracted from proton scattering [20–22] which yields a partial $E3$ lifetime of approximately 120 ps and a ground-state branch of less than 0.1%.

Because the two lineshapes overlapped it was necessary for all rings to be analyzed simultaneously, with the backward rings being particularly sensitive to short $3_{(2)}^-$ lifetimes and the forward rings placing limits on long lifetimes. Simulated spectra were again generated with $5 \cdot 10^6$ CsI(Tl)- γ coincident events, with the feeding and subsequent decay of the 2_1^+

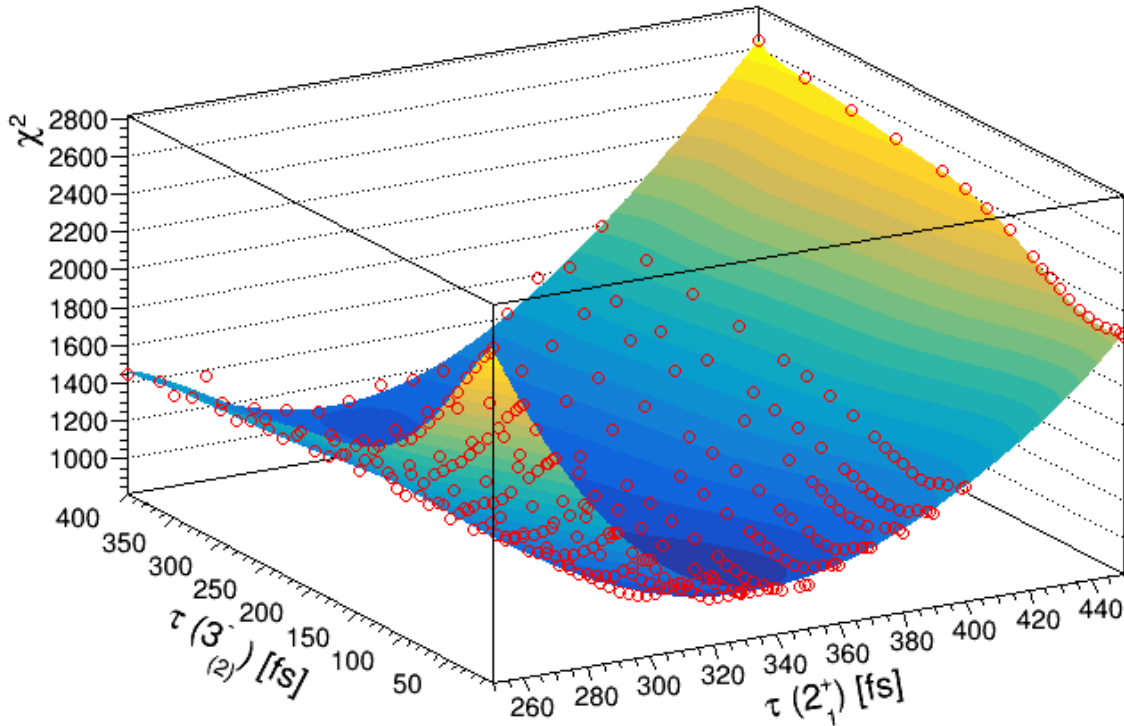


FIG. 6. The χ^2 surface fitted to the minimized χ^2 values (red circles) used to determine the lifetime minima for the overlapping 2_1^+ and $3_{(2)}^-$ lineshapes.

state included in the simulation of the 3^- decay (see Ref. [18]). 340 simulated data sets were therefore created for the 3^- decay, corresponding to seventeen potential 2_1^+ lifetimes and twenty potential $3_{(2)}^-$ lifetimes, with a further seventeen simulated datasets corresponding to direct population of the 2_1^+ state. Feeding of the 2_1^+ state from the stopped ($t_{1/2}=3.1$ ns) 4_1^+ state was also simulated. Feeding from the 2_2^+ state was included but was found to have very little effect on the final result.

The simulated data were then fit to the experimental spectra, with all four rings fitted simultaneously. For each ring, the following parameters were independently varied to achieve the best fit: a scaling parameter for the 2_1^+ direct feeding, a scaling parameter for the $3_{(2)}^+$ decay (including the resultant decay of the 2_1^+ state), a zeroth order polynomial background and an E_γ -shift parameter to allow for low-level mismatch between simulated and experimental energies. The 4^+ feeding contribution was fixed for all rings based on a fit to the intensity of the $4_1^+ \rightarrow 2_1^+$ decay line.

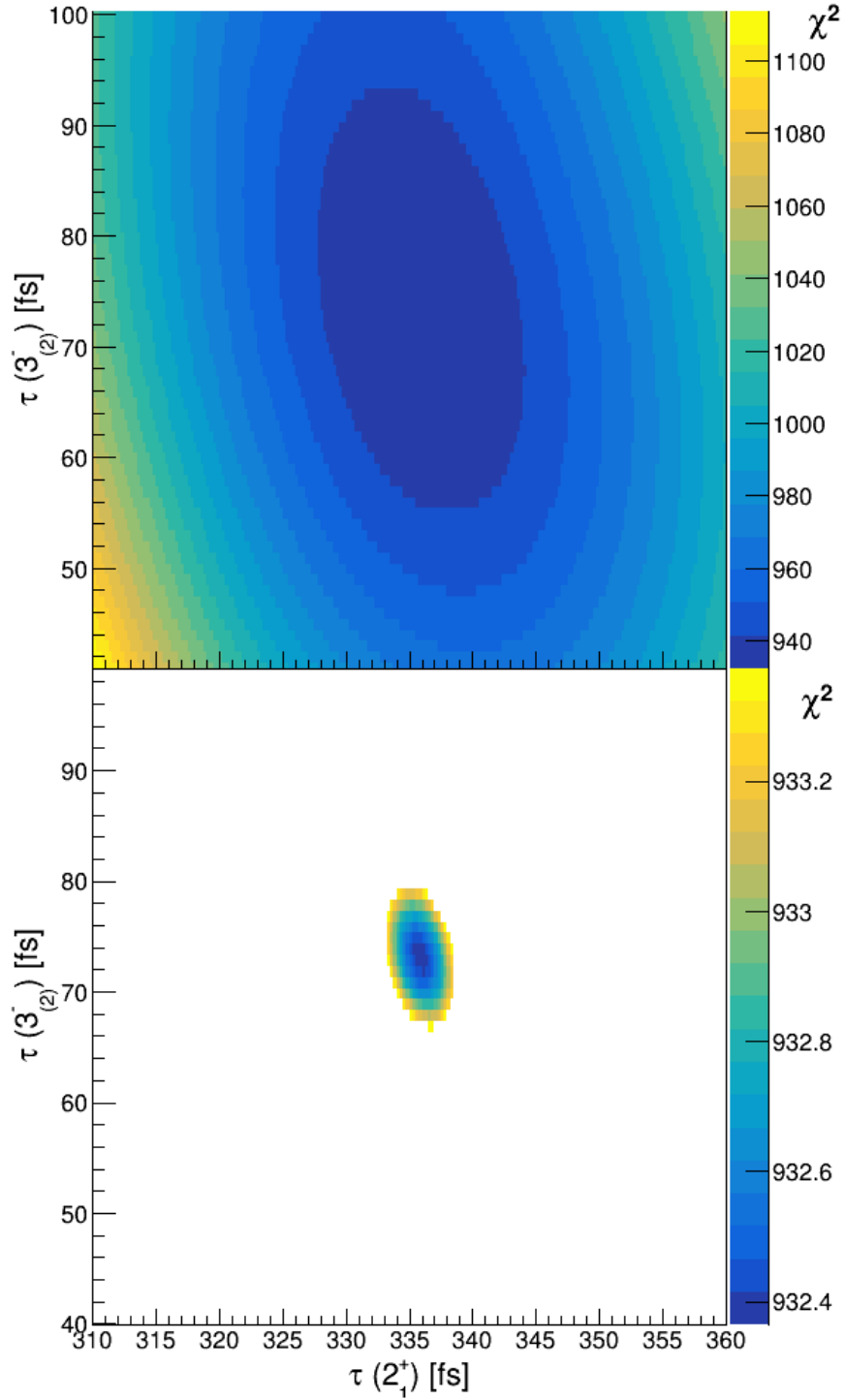


FIG. 7. Top: χ^2 surface as determined from the fit shown in Fig. 6 in the region of χ^2_{\min} . Bottom: The $\chi^2 \leq \chi^2_{\min} + 1$ region from which the minimum and associated statistical uncertainties were determined.

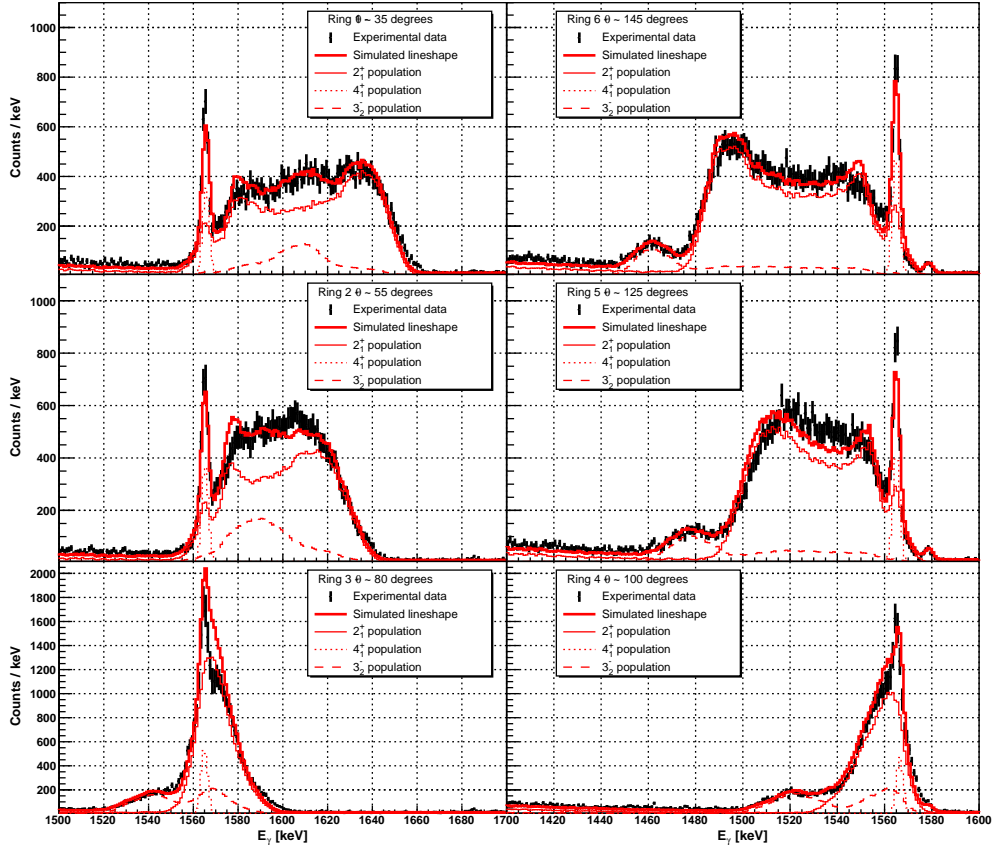


FIG. 8. Fitted lineshape (thick solid, red) corresponding to the minimized χ^2 overlaid on the experimental data (black points) for the six rings in TIGRESS. Also shown are the primary contributions to the lineshape arising from direct population of the 2_1^+ state (thin solid, red), population via the 4_1^+ state (dotted, red) and via the $3_{(2)}^-$ state (dashed, red). Details of the parameters varied in the fits are provided in the text. Rings 3 and 4 were insensitive to the state lifetimes and were not included in the χ^2 surface shown in Fig. 6.

A χ^2 surface was fit to the resultant χ^2 values, as shown in Fig. 6. From this, the $\chi_{min}^2 \leq \chi^2 \leq \chi_{min}^2 + 1$ range could then be extracted to determine the resultant state lifetimes and their associated uncertainties. Figure 7 shows the total and 1σ surface in the vicinity of the minimum with the fitted lineshapes shown in Fig. 8, along with the major contributions to the fit. The resultant lifetimes are $\tau(2_1^+) = 336 \pm 3$ fs and $\tau(3_{(2)}^-) = 73 \pm 5$ fs. To account for the fact that the reduced $\chi_{min}^2/\nu = 1.6 > 1$, the statistical uncertainties were inflated by a factor of $\sqrt{\chi_{min}^2/\nu} = 1.3$ following the prescription of Ref. [19], yielding final lifetimes of $\tau(2_1^+) = 336$ fs with $\delta\tau_{stat}(2_1^+) = 4$ fs and $\tau(3_{(2)}^-) = 73$ fs with $\delta\tau_{stat}(3_{(2)}^-) = 6$ fs.

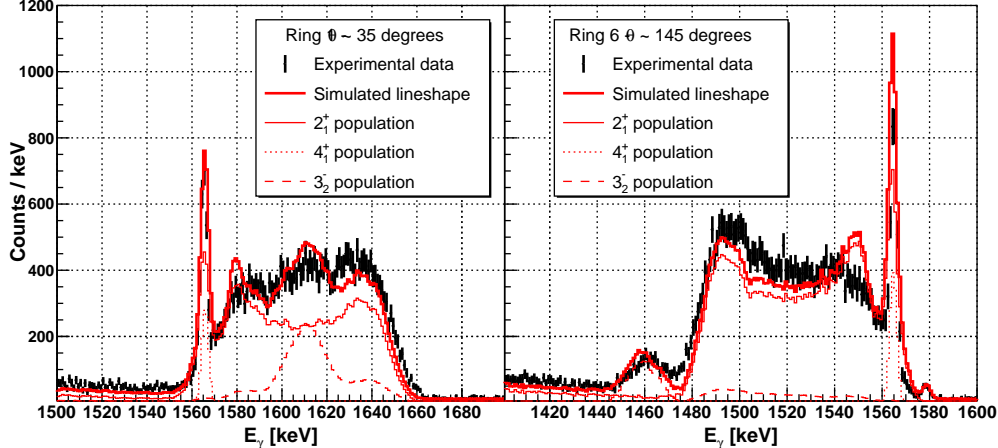


FIG. 9. Lineshapes for a 2_1^+ state lifetime of 450 fs (Ref. [7]: $\tau(2_1^+) = 440(25)$ fs) for the downstream- and upstream-most rings. A $3_{(2)}^-$ state lifetime of $\tau(3_{(2)}^-) = 10$ fs is used, corresponding to the approximate χ^2 minimum in Fig. 6 at $\tau(2_1^+) = 450$ fs. The poorer quality of the fit for both the 2_1^+ and 3^- components is clear in comparison to that of Fig. 8.

C. Systematic uncertainties

Uncertainties on the present measurement are dominated by systematic effects. The primary systematic uncertainties in the present measurement arise from uncertainties in the stopping powers for krypton in amorphous carbon and gold. The fast (large v/c) component to the lineshapes was found to be sensitive to the stopping in carbon and was varied during the simulation procedure. All results thus far correspond to a stopping power of 60% of that included by default within the GEANT4 libraries which was found to best reproduce the data. Full simulations were performed for 40%, 50%, 60%, 70% and 80% of the nominal carbon stopping powers in GEANT4. Based on simulations performed with these stopping powers systematic uncertainties of $\delta\tau(2_1^+) = 7$ fs and $\delta\tau(3_{(2)}^-) = 4$ fs were estimated. A similar analysis was performed for the lifetime of the 2_2^+ state, yielding an uncertainty from the carbon stopping powers of $\delta\tau(2_2^+) = 5$ fs. No clear sensitivity was discernible in the fitting to the stopping of krypton in gold. We attribute a 5% additional systematic uncertainty to the final results from potential discrepancies in gold stopping powers. A small systematic uncertainty (2 fs) is also associated with the choice of polynomial used to fit the χ^2 surface in Fig. 6. We find a small sensitivity to feeding from the 2_2^+ state, from which we attribute a 1 fs systematic uncertainty to the 2_1^+ and 3^- lifetimes. Finally, it is found that for the

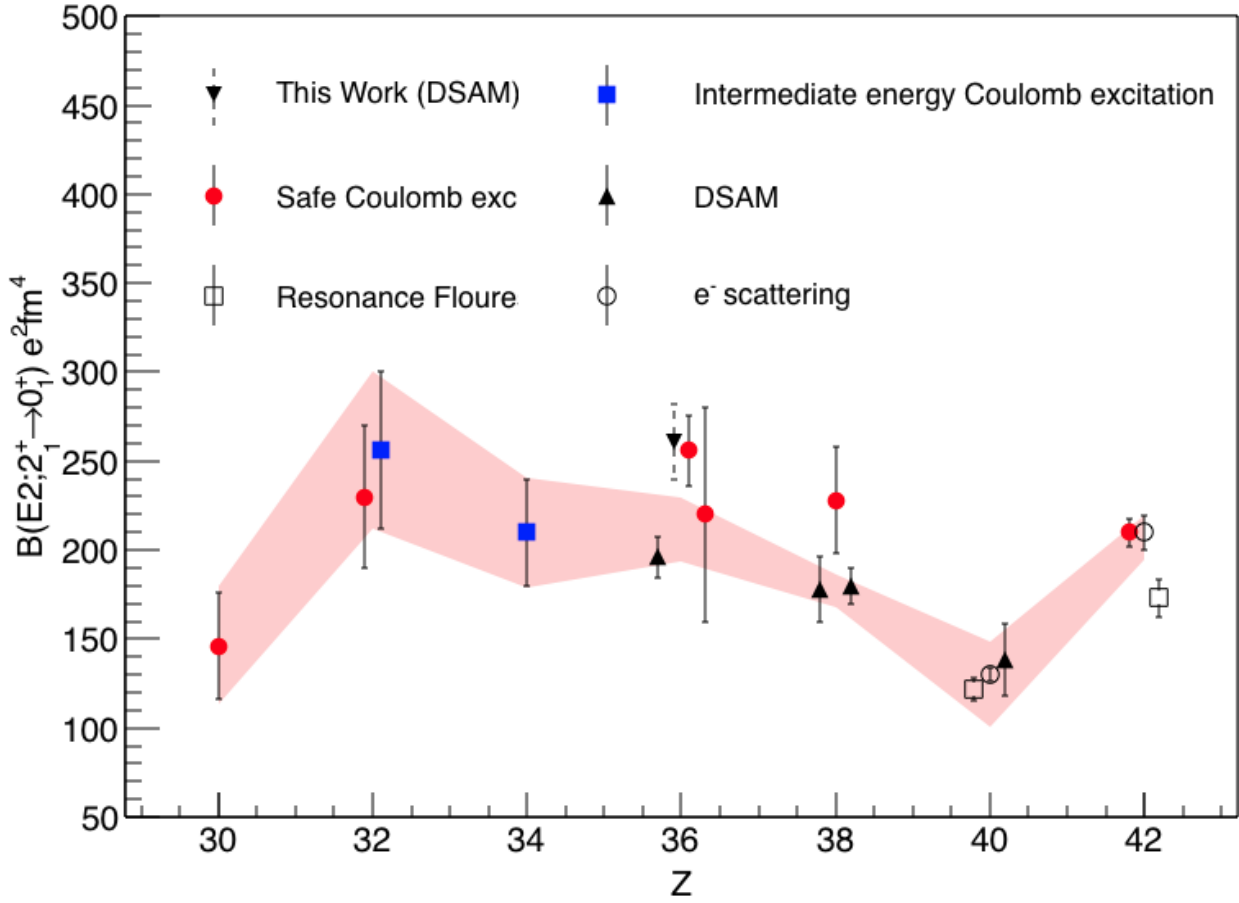


FIG. 10. $B(E2; 2_1^+ \rightarrow 0_1^+)$ value systematics for the $N = 50$ isotones. The uncertainties on the present result are dominated by systematics (dashed lines) but agree well with previous Coulomb excitation data. The evaluated data range is indicated by the shaded band. Experimental data taken from Refs. [7, 8, 23–35].

$3_{(2)}^-$ state there is a discrepancy between the lifetime extracted using rings one and six (35° and 145° , 96 (10) fs), and that extracted using rings two and five (55° and 125° , 53 (11) fs). We attribute a 20 fs systematic uncertainty, accordingly. The equivalent discrepancy for the 2_1^+ and 2_2^+ states is found to be approximately 2 fs. We therefore quote final systematic uncertainties of $\delta\tau_{(\text{sys.})}(2_1^+) = 20$ fs, $\delta\tau_{(\text{sys.})}(2_2^+) = 19$ fs and $\delta\tau_{(\text{sys.})}(3_{(2)}^-) = 32$ fs, giving results of $336 \pm 4(\text{stat.}) \pm 20(\text{sys.})$ fs for the 2_1^+ state, $263 \pm 9(\text{stat.}) \pm 19(\text{sys.})$ fs for the 2_2^+ state, and $73 \pm 6(\text{stat.}) \pm 32(\text{sys.})$ fs for the $3_{(2)}^-$ state.

TABLE I. Lifetimes and reduced transition probabilities as determined in the present work compared to literature values, where available. The branching ratio of the 2_2^+ state was taken from Ref. [36]. The quoted $B(E1)$ for the $3^- \rightarrow 2^+$ transition assumes a pure $E1$. No other decay branches for the $3_{(2)}^-$ state are known, nor were any observed in the present work. Here, the first quoted uncertainty corresponds to statistics, the second to systematics.

Transition	τ (fs)		$B(E\lambda)$ e ² fm ^{2λ}		
	This Work	Lit.	This Work	Lit.	Ref.
$2_1^+ \rightarrow 0_1^+$	336 (4)(20)	444 (25)	259 (3)(16)	196 (11)	[7]
		341 (27)		256 (20)	[8]
		396 (108)		220 (60)	[26]
$3_{(2)}^- \rightarrow 2_1^+$	73 (6)(32)		0.0024 (2)(11)		
$2_2^+ \rightarrow 0_1^+$	263 (9)(19)		31 (1)(2)		
$2_2^+ \rightarrow 2_1^+$	263 (9)(19)		<3000		

Transition	τ (fs)	$B(M1)$ μ_N^2
$2_2^+ \rightarrow 2_1^+$	263 (9)(19)	< 0.13

IV. DISCUSSION

The present results deviate from those determined in Ref. [7] by more than three standard deviations. We note, however, that the measurement reported in Ref. [7] was unable to resolve the 3^- state observed in the present work. The failure to include this contribution in the lifetime determination of the present work - even at relatively low levels - would result in the extraction of a longer lifetime from the analysis. This highlights the importance of using HPGe arrays with detectors at both forward and backward angles in DSAM analyses. In order to demonstrate to the reader the incompatibility of the lifetime quoted in Ref. [7] with the present data, Fig. 9 shows simulated lineshapes corresponding to a lifetime of 450 fs. The lifetime extracted in the present work is in good agreement with both the Coulomb excitation works of Ref. [8] and Ref. [26]. Excluding the DSAM result of Ref. [7] for the

above stated reasons, we determine a new weighted average lifetime, $\tau_{2_1^+} = 339 \pm 16$ fs.

Figure 10 shows $B(E2; 2_1^+ \rightarrow 0_1^+)$ values for the $N = 50$ isotones, where known. Clearly, the present result and its associated conclusions represents a significant deviation from the accepted values, with ^{86}Kr now becoming one of the more collective of the $N = 50$ nuclides. In light of the present result, a remeasurement of the $B(E2; 2_1^+ \rightarrow 0_1^+)$ value in ^{88}Sr would be of interest in order to confirm behaviour approaching $Z = 40$.

V. CONCLUSIONS

We have remeasured the lifetime of the first-excited state in ^{86}Kr using the Doppler-shift attenuation method (DSAM) following population in unsafe Coulomb excitation. Our result agrees with previous Coulomb-excitation measurements and disagrees with a previous DSAM measurement at the 3σ level. We hypothesize that this discrepancy may arise from the failure of the previous measurement to resolve a feeding state with a lineshape that overlaps with the state of interest. We were further able to extract lifetimes for the $3_{(2)}^-$ and 2_2^+ states and determine transition strengths accordingly. Our new data indicate a more precipitous reduction in $B(E2)$ strength in the $N = 50$ isotones approaching the $Z = 40$ sub-shell closure than was previously thought to occur. This new lifetime may also affect the conclusions of g-factor measurements which need to account for the lifetimes of the states of interest (e.g. Ref. [7] and Ref. [29]) in the transient-field technique.

VI. ACKNOWLEDGEMENTS

The authors would like to thank the TRIUMF beam delivery group for their efforts in providing high-quality beams. This work has been supported by the Natural Sciences and Engineering Research Council of Canada (NSERC), The Canada Foundation for Innovation and the British Columbia Knowledge Development Fund. TRIUMF receives federal funding via a contribution agreement through the National Research Council of Canada. The work at LLNL is under contract DE-AC52-07NA27344.

[1] A. Navin et al. *Physical Review Letters*, 85:266, 2000.

- [2] C. Thibault et al. *Physical Review C*, 12:644, 1974.
- [3] B. Bastin et al. *Physical Review Letters*, 99:022503, 2007.
- [4] S. Naimi et al. *Physical Review C*, 86:014325, 2012.
- [5] C. Santamaria et al. *Physical Review Letters*, 115:192501, 2015.
- [6] F. Nowacki et al. *Physical Review Letters*, 117:272501, 2016.
- [7] T. J. Mertzimekis et al. *Physical Review C*, 64:024314, 2001.
- [8] J. Cheng-Lie and S. Pontoppidan. *Physical Review C*, 24:1350, 1981.
- [9] A. Chester et al. *Nuclear Instruments and Methods in Physics Research A*, 882:69, 2018.
- [10] K. Jayamanna et al. *Review of Scientific Instruments*, 79:2, 2008.
- [11] G. Hackman and C. E. Svensson. *Hyperfine Interactions*, 225:241, 2014.
- [12] P. Voss et al. *Nuclear Instruments and Methods in Physics Research A*, 746:87, 2014.
- [13] J. Greene, P. Voss, and K. Starosta. *Journal of Radioanalytical and Nuclear Chemistry*, 299:1121, 2014.
- [14] J. P. Martin, C. Mercier, N. Starinski, C. J. Pearson, and P. A. Amaudruz. *IEEE Trans. Nucl. Sci*, 55:84, 2008.
- [15] P. Voss et al. *Physical Review C*, 96:024305, 2017.
- [16] GRSISort. <https://github.com/GRIFFINCollaboration/GRSISort/>.
- [17] R. Brun and F. Rademakers. *Nucl. Instr. Meth. in Phys. Res. A*, 389:81, 1997.
- [18] J. Williams et al. *Nuclear Instruments and Methods in Physics Research A*, 850:8, 2017.
- [19] C. Patrignani et al. *Review of Particle Physics, Chinese Physics C*, 40.
- [20] T. Kibédi and R. H. Spear. *Atomic Data and Nuclear Data Tables*, 80:35, 2002.
- [21] B. K. Arora et al. *Physical Review C*, 10:2301, 1974.
- [22] S. Matsuki et al. *Physics Letters B*, 72:319, 1978.
- [23] J. van der Walle et al. *Physical Review Letters*, 99:142501, 2007.
- [24] E. Padilla-Rodal et al. *Physical Review Letters*, 94:122501, 2005.
- [25] A. Gade et al. *Physical Review C*, 81:064326, 2010.
- [26] C. M. Cartwright, P. D. Forsyth, I. Hall, A. D. Irving, and D. G. E. Martin. *Journal of Physics G*, 7:65, 1981.
- [27] A. I. Kucharska, J. Billowes, and M. A. Grace. *Journal of Physics G*, 14:65, 1988.
- [28] P. R. Christensen et al. *Nuclear Physics A*, 207:433, 1973.

- [29] G. J. Kumbartzki et al. *Physical Review C*, 89.
- [30] J. Heisenberg et al. *Physical Review C*, 29:97, 1984.
- [31] F. R. Metzger. *Nuclear Physics A*, 182:213, 1972.
- [32] G. P. S. Sahota at others. *Journal of the Physical Society of Japan*, 62:2958, 1993.
- [33] S. Raman et al. *Atomic Data and Nuclear Data Tables*, 36:1.
- [34] F. R. Metzger. *Physical Review C*, 15:193, 1977.
- [35] T. E. Milliman. PhD thesis, University of New Hampshire, 1987.
- [36] NNDC. Evaluated Nuclear Structure Data File (ENSDF).